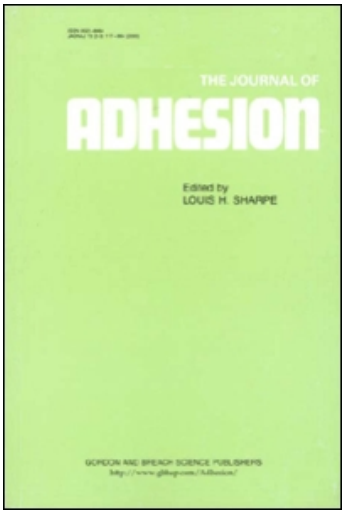

The Journal of Adhesion
Publication details, including instructions for authors and subscription information:
http://www.informaworld.com/smpp/title~content=t713453635

Analytical Peel Load Prediction as a Function of Adhesive Stress Concentration

R. X. Wang[a]; A. Shayganpur[a]; S. Sareskani[a]; J. K. Spelt[a]
[a] Department of Mechanical and Industrial Engineering, University of Toronto, Toronto, Ontario, Canada

To cite this Article Wang, R. X. , Shayganpur, A. , Sareskani, S. and Spelt, J. K.(2006) 'Analytical Peel Load Prediction as a Function of Adhesive Stress Concentration', The Journal of Adhesion, 82: 1, 39 — 61
To link to this Article: DOI: 10.1080/00218460500418599
URL: http://dx.doi.org/10.1080/00218460500418599

The Journal of Adhesion, 82:39–61, 2006

ISSN: 0021-8464 print/1545-5823 online
DOI: 10.1080/00218460500418599

Taylor & Francis
Taylor & Francis Group

Analytical Peel Load Prediction as a Function of Adhesive Stress Concentration

R. X. Wang
A. Shayganpur
S. Sareskani
J. K. Spelt
Department of Mechanical and Industrial Engineering,
University of Toronto, Toronto, Ontario, Canada

Peel data for two epoxy adhesives and a recent model of the adhesive stresses in the peel geometry are used to investigate the effectiveness of two constitutive models and several adhesive failure criteria. The failure criteria are based on either the critical strain energy-release rate or the critical von Mises strain at the peel root, both taken as functions of the "loading zone length" (LZL)*, defined as a measure of the degree of stress concentration at the root of the peeling adherend. The peel model uses* LZL *as an independent parameter that captures the effects of the peel angle, adherend thickness, and the mechanical properties of the adhesive and adherend. Both the energy- and strain-based failure criteria can be used to predict the steady-state peel load with an average absolute error of less than 10% over the range of conditions that were examined.*

Keywords: Adhesive; Epoxy; Fracture; Model; Peel; Prediction; Strain; Stress

1. INTRODUCTION

The failure of adhesive joints with relatively thin metal adherends is often accompanied by extensive plastic deformation of the metal. A common example is the typical peel test. In such cases, the identification of a failure criterion and the ability to predict joint strength are complicated by the strong dependence of the adhesive stress state

Received 25 January 2005; in final form 9 July 2005.
Presented in part at the 27th Annual Meeting of the Adhesion Society, Wilmington, North Carolina, USA, 15–18 February 2004.
Address correspondence to Jan K. Spelt, University of Toronto, Department of Mechanical and Industrial Engineering, 5 King's College Road, Toronto, Ontario M5S 3G8, Canada. E-mail: spelt@mie.utoronto.ca

on the deformed adherend geometry in the vicinity of the peel root where the adhesive is breaking.

In cases where the adherends remain elastic, the failure of relatively brittle structural adhesives can be predicted using the critical strain energy-release rate as a function of the mode ratio of loading [1]. When metal adherends deform plastically at the adhesive crack tip, the degree of stress concentration in the adhesive and, hence, the stress state and the volume of load-bearing adhesive vary with the peel load and angle, as well as with the mechanical properties of the adherend and adhesive. In an earlier article, it was suggested that this makes the critical strain energy-release rate a function of the stress concentration in the adhesive layer as well as of the mode ratio of loading [2, 3].

The analysis of adhesive peeling is a complex subject that has been the subject of numerous studies (see, for example, the reviews in Refs. 2 and 3). Lately, there has been considerable attention paid to cohesive zone models of the adhesive fracture behavior in the vicinity of the peel root [4, 5]. This approach has the virtue of capturing the essential load-deformation response of the adhesive in a simplified model that avoids the detailed consideration of the fracture mechanics at the adhesive crack tip.

The present article investigates several adhesive failure criteria using peel data for two epoxy adhesives and a recent model of the adhesive stresses in the peel geometry [2, 3]. The failure criteria are based on either the critical strain energy-release rate or the critical von Mises strain at the peel root, both taken as functions of the degree of stress concentration at the root.

2. EXPERIMENTS

Flexible-to-rigid peel joints were made with various thicknesses of AA5754-O aluminum sheet (1, 2, and 3 mm) bonded to a rigid aluminum plate (AA6061-T6, 12.5 mm thick) using the single-part heat-cured epoxy adhesives Betamate® 1044-3 and Betamate® 4601 (Essex Specialty Products Inc., Auburn Hills, MI, USA). The sheets (90×430 mm) and plates (90×320 mm) were degreased with acetone, washed with Alumiprep 33, and then pretreated with Alodine 5200 chrome-free conversion coating (Henkel Surface Technologies, Madison Heights, MI, USA). The sheets and plates were bonded such that a 110-mm length of sheet extended beyond the joint and could be gripped during the peel test. The bondline thickness was controlled at 0.4 mm using polytetrafluoroethylene shims, and both adhesives were cured at 180°C for at least 1 h. Each of the bonded sheet–plate joints was then cut slowly into three peel specimens, 20 mm wide,

TABLE 1 Measured and Predicted Peel Loads with the Percentage Error for the Two Failure Criteria (85% *LZL*); Betamate 1044; Adhesive Continuum Model (CM)

Adherend thickness (mm)–peel angle (deg)	Measured peel force (N/mm), standard deviation, no. measurements	Predicted peel force (N/mm) with $G_c(LZL)$, % error	Predicted peel force (N/mm) with $\varepsilon_c(LZL)$, % error
1–30	35.2, 0.12, 2	34.7, –1.4	33, –6.3
1–60	12.1, 0.32, 2	12.2, 0.8	12.7, 5.0
1–90	6.82, 0.42, 2	7.0, 2.6	7.0, 2.6
2–30	50.7, 2.44, 4	53.4, 5.3	51.9, 2.4
2–60	16.2, 1.97, 4	16.7, 3.1	17.7, 9.3
2–90	8.43, 0.79, 4	9.4, 12	9.2, 9.1
3–30	68.4, 1.79, 4	69.0, 0.9	67.9, –0.7
3–60	20.8, 1.72, 4	20.4, –1.9	22.1, 6.3
3–90	12.2, 2.00, 4	11.3, –7.4	11.3, –7.4

using a table saw or milling machine with an aqueous coolant spray. The exposure to the coolant was too brief for any appreciable absorption, and there was no evidence of edge damage on the peeled surfaces.

The specimens were peeled at 2.5 mm/min using a sliding fixture to maintain the peel angle [3]. The first and second columns of Tables 1

TABLE 2 Measured and Predicted Peel Loads with the Percentage Error for the Two Failure Criteria (85% *LZL*); Betamate 4601; Adhesive Continuum Model (CM)

Adherend thickness (mm)–peel angle (deg)	Measured peel force (N/mm), standard deviation, no. measurements	Predicted peel force (N/mm) with $G_c(LZL)$, % error	Predicted peel force (N/mm) with $\varepsilon_c(LZL)$, % error
1–30	26.4, 2.4, 4	32.2, 22	30.7, 16
1–45	13.4, 0.7, 6	15.5, 16	16, 19
1–60	8.7, 0.5, 4	9.9, 14	9.8, 13
1–90	4.6, 0.4, 5	5.5, 20	5.1, 11
1–120	3.2, 0.3, 5	4, 29	3.3, 6.5
2–30	54.8, 4.4, 8	56.4, 2.9	52.7, –3.8
2–45	29.9, 0.4, 4	25.7, –14	27.7, –7.4
2–60	18.0, 0.8, 5	14.9, –17	16.3, –9.4
2–90	9.9, 0.9, 5	7.9, –20	8, –19
3–30	73.1, 6.6, 4	82.15, 12	73.5, 0.5
3–45	35.5, 1.9, 3	34.7, –2.3	37.7, 6.2
3–60	19.6, 1.7, 3	20.2, 3.1	22.7, 16
3–90	10.7, 0.8, 6	10.8, 0.9	10.8, 0.9

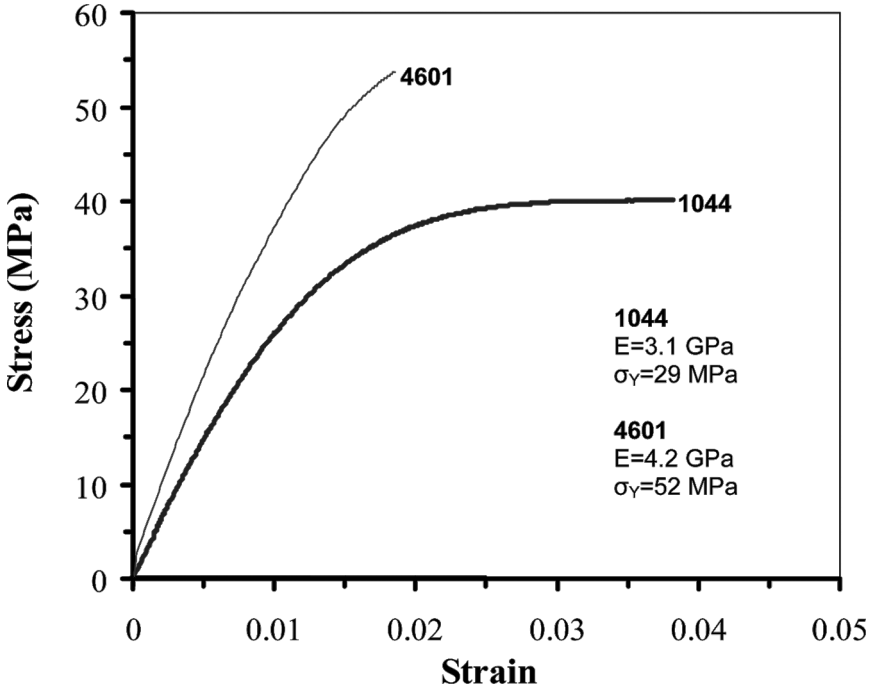

FIGURE 1 Tensile stress–strain curves with measured Young's modulus and yield stress for epoxy adhesives Betamate® 1044 and Betamate® 4601 (Essex).

and 2 list the peel cases for each adhesive (peel strip thickness and peel angle, θ) and the measured average peel force (together with the standard deviation and the number of measurements). As mentioned, the data for the 1044 adhesive (Table 1) were used in developing the models of Ref. 3. The 4601 adhesive had a higher modulus and yield strength but was less ductile than the 1044 adhesive (Figure 1). The aluminum alloy (AA5754-O) exhibited elastic–plastic behavior with $E_{\text{el}} = 71.0\,\text{GPa}$ and $E_{\text{pl}} = 0.483\,\text{GPa}$ for the elastic and plastic moduli, respectively, and $\sigma_{\text{yp}} = 100\,\text{MPa}$ for the yield stress. Two additional peel angles were measured with the 4601 adhesive: 45° and 120° [6].

3. PEEL MODEL

The present peel model for the stresses in the adhesive layer of a peeling strip was described in detail in Refs. 2 and 3. It is based on the adhesive sandwich model of Crocombe and Bigwood [7], which was extended to include the shear deformation of the adherends [2].

The model accommodates arbitrary loading, a bilinear adherend stress–strain response, and any form of nonlinear adhesive behavior. By changing the boundary conditions at the ends of the sandwich adherends (right part of Figure 2), the model may be used to analyze many two-dimensional joints in which adherends yield. In the present case, the sandwich model was coupled to an existing analytical model for the detached adherend in a flexible–rigid peel specimen (Figure 2), thereby allowing for the investigation of several failure criteria using peel test data [3].

In the present work, two constitutive adhesive models were evaluated for their ability to represent the behavior of the adhesive: 1) a continuum model (CM) under various levels of constraint (plane stress, plane strain, uniaxial strain) was applied to the peel data of both adhesives, and 2) a cohesive zone model (CZM) was used to represent the Betamate 1044 adhesive in the vicinity of the crack tip at the root of the peeling strip (data were unavailable to apply the CZM to the Betamate 4601 adhesive). The continuum model of the adhesive was the same as that used in Refs. 2 and 3 in which the adhesive stress–strain response was modeled using a spline fit

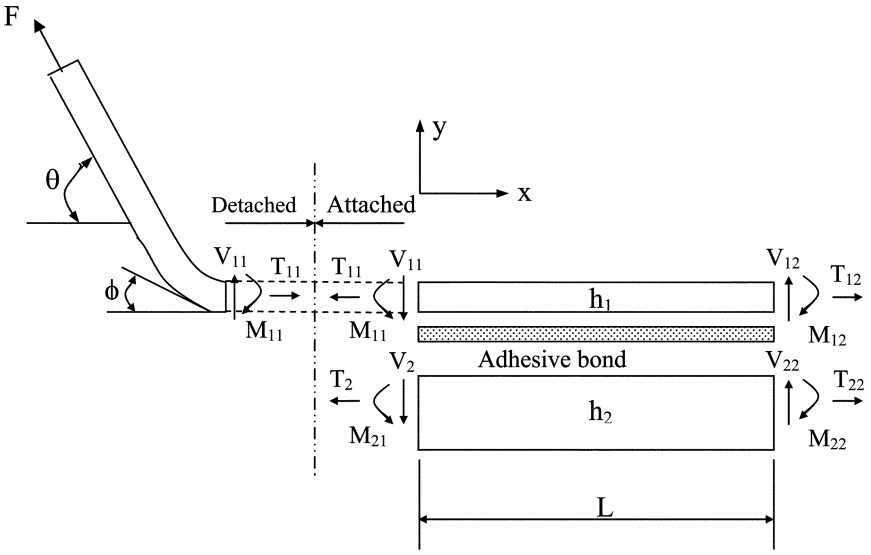

FIGURE 2 Free-body diagram of peel specimen illustrating merging of separate analyses of sandwich element and detached peel strip of thickness h_1. Adherends treated as beams subject to arbitrary bending (M), tensile (T), and shear (V) loads acting on each cross section. Peel angle θ and root rotation angle φ.

to the experimental curve (Figure 1). The true value of the ultimate adhesive stress and strain in the tensile tests (Figure 1) is uncertain because failure is strongly influenced by the presence of small defects in the specimen gauge section. In constructing the adhesive constitutive model, it was assumed that the adhesive stress remained constant beyond the ultimate strains shown in Figure 1. In all peel models, the peeling adherend (5754-O) was modeled as a bilinear material as described. For the continuum model, the critical energy-release rate, G_c, was calculated as the difference between the work per unit debonded area done by the peel force and the energy per unit area dissipated by plastic bending in the detached peel adherend [2, 3].

The cohesive zone model of the Betamate 1044 adhesive used the tensile and shear traction–separation curves shown in Figure 3, in which δ_n and δ_t are the normal and shear displacements across the adhesive layer. The cohesive zone parameters of these curves were determined by using the sandwich model [2] to fit elastic mixed-mode double-cantilever-beam (DCB) fracture data for the 1044 adhesive. The areas under the two curves, Γ_{OI} and Γ_{OII}, were taken to be equal to the mode I and II critical energy-release rates of the adhesive, G_{Ic} and G_{IIc}, respectively, from DCB measurements [8, 9]. The rising slopes were calculated from the measured tensile and shear moduli of the adhesive, E and G, respectively. The remaining adjustable parameters were the maximum tensile and shear tractions, $\hat{\sigma}$ and $\hat{\tau}$, which were selected to best fit the mixed-mode DCB fracture data. The relationships among the independent parameters of Figure 3 are

$$\Gamma_{\mathrm{OI}} = \frac{1}{2}\delta_{\mathrm{nc}}\hat{\sigma}, \tag{1}$$

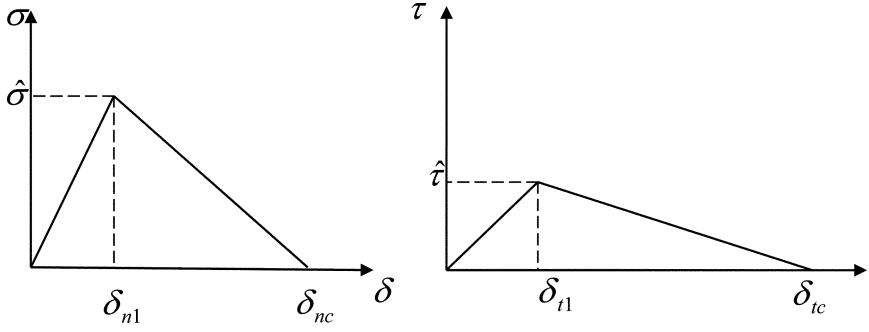

FIGURE 3 Stress-deflection response of tension (σ) and shear (τ) springs used in adhesive layer cohesive zone model (CZM).

$$\Gamma_{\mathrm{OII}} = \frac{1}{2}\delta_{\mathrm{tc}}\hat{\tau}, \tag{2}$$

$$\frac{\delta_{n1}}{t} = \frac{\hat{\sigma}}{E}, \tag{3}$$

$$\frac{\delta_{t1}}{t} = \frac{\hat{\tau}}{G}, \tag{4}$$

where t is the thickness of the adhesive layer.

The traction–separation relations of Figure 3 were used to establish expressions for the adhesive tensile stress in the y-direction, $\sigma = f(\varepsilon)$, and the adhesive shear stress, $\tau = g(\gamma)$, which were then substituted into the first three of the six differential equations governing the continuum model [2]. Assuming plane strain in the adhesive layer, this yields

$$\frac{dT}{dx} = \tau = g(\gamma), \tag{5}$$

$$\frac{dV_1}{dx} = \sigma = f(\varepsilon), \tag{6}$$

$$\frac{dM_1}{dx} = V_1 - \frac{(h_1 + t)}{2}\tau. \tag{7}$$

The continuum model computer code was then modified slightly to handle these new constitutive relations. As mentioned previously, for the cohesive zone model, G_c was calculated as the sum of the areas under the mode I and mode II traction separation curves when the peeling load is attained.

4. FAILURE CRITERIA

The objective of this work was to use the peel model of Ref. 2 to identify a failure criterion that could be expressed in terms of an independent parameter that captures the combined effect of peel angle and peel strip thickness. In Ref. 3 it was found that the critical strain energy-release rate, G_c, increased linearly with the average phase angle, φ (the average of the local phase angle over the adhesive layer defined below as Eq. [11]), for the nine Betamate 1044 peel cases given in the first column of Table 1. Furthermore, the average phase angle increased linearly with a measure of the stress concentration in the adhesive, the LZL, defined arbitrarily as the distance in the x-direction of Figure 2 from the peel root to the point in the adhesive

where the von Mises stress was 15% of that at the root [3]. Therefore, a linear correlation $G_c(\varphi)$ implies a linear correlation $G_c(LZL)$, which is consistent with the present hypothesis that, in situations with extensive adherend plastic deformation, G_c should be a function of the phase angle (as it is in fracturing adhesive joints without adherend yielding) and the degree of stress concentration near the adhesive crack tip.

4.1. Failure Criteria Used with Adhesive Continuum Model

In the present article, the LZL was developed further as an independent parameter for use in the prediction of peel force for arbitrary combinations of peel angle and strip thickness. Two failure criteria were investigated as functions of LZL with the continuum adhesive model: The first used $G_c(LZL)$ for which LZL was defined arbitrarily as the length of the adhesive layer in the x-direction (Figure 2) from the root to the point where the von Mises stress was 15% of its maximum value at the root (as in Ref. 3). The second failure criterion used the critical von Mises strain, ε_c, at the crack tip (peel root) as a function of an LZL defined, in this case, as the length of the adhesive layer from the root to the point where the von Mises strain was 15% of its value at the root, ε_c. For both failure criteria, the peel load was predicted using an iterative search: the load on the peel strip was incremented and new values of G, ε, and LZL were calculated and compared with the failure criteria. The iterations stopped when the incremented peel strip load had been identified as the critical load for which the calculated G or ε was equal to the corresponding G_c or ε_c, depending on the failure criterion. This process is illustrated in Figure 4, which shows how G increases with LZL as the load on the peel strip is iteratively incremented for the 1-mm-30° and 3-mm-30° cases. It is seen that the trajectory of $G(LZL)$ intersects the failure criterion line, $G_c(LZL)$, at an angle that is sufficiently large to ensure an efficient convergence to the predicted peel load.

As is discussed later, the phase angle of the loading proved to be an ineffective independent parameter for peel load prediction because of the relatively weak dependence of the strain energy-release rate on the phase angle.

4.2. Failure Criteria Used with Adhesive Cohesive Zone Model

The CZM of the adhesive was investigated using two energy based criteria: 1) $G_c(LZL)$ with a normal displacement-based definition of LZL, and 2) a criterion based on the strain energy mode mix using the same normal displacement-based definition of LZL. In the first

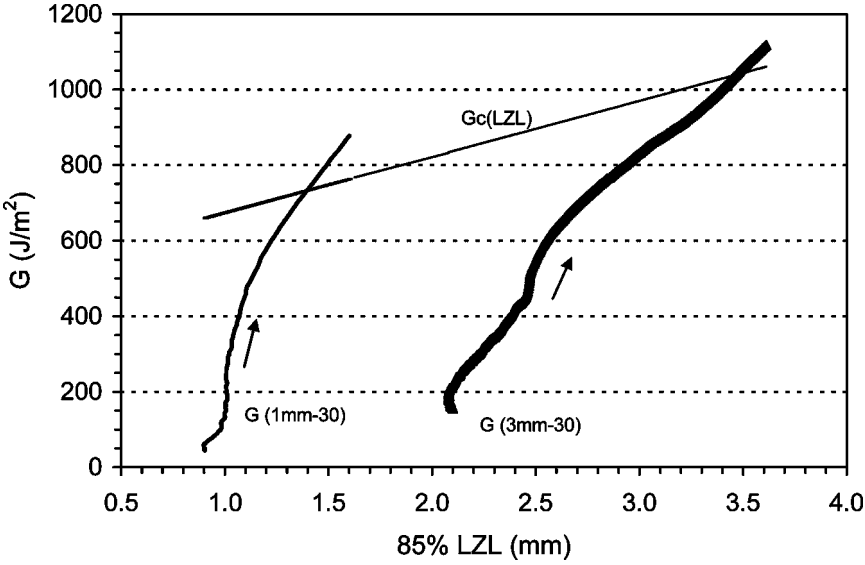

FIGURE 4 Trajectory of $G(LZL)$ as the load applied to the peel strip is iteratively increased for the 1 mm–30° and 3 mm–30° peel 1044 cases. The straight line is the $G_c(LZL)$ failure criterion (Figure 6a). Arrows indicate the trajectory direction as peel load is increased.

failure criterion, adhesive failure was predicted when the sum of the strain energies in tension and shear at the peel root (*i.e.*, the areas under the curves of Figure 3 corresponding to the adhesive tensile and shear deformations at the root δ_n and δ_t, respectively) equaled the critical strain energy-release rate obtained from the peel data; *i.e.*, $G_{\mathrm{I}} + G_{\mathrm{II}} = G_c(LZL)$. The independent parameter was LZL; however, in this case it was defined as the distance from the peel root to the point where the adhesive tensile displacement (δ_n) was 15% of its value at the root.

The second failure criterion was a simple, well-known mixed-mode fracture criterion:

$$\lambda = \frac{G_{\mathrm{I}}}{\Gamma_{\mathrm{OI}}} + \frac{G_{\mathrm{II}}}{\Gamma_{\mathrm{OII}}} \tag{8}$$

where, as previously, G_{I} and G_{II} represent the mode I and mode II traction–separation work absorbed by the fracture process, respectively.

$$G_{\mathrm{I}} = \int_0^{\delta_n^p} \sigma(\delta_n) d\delta_n \tag{9}$$

TABLE 3 Adhesive Constitutive Models and Failure Criteria

Adhesive constitutive models	Adhesive failure criteria with definition of LZL	
	X	**X**
Continuum model (CM)	$G_c(LZL)$—85% decrease in von Mises stress	$\varepsilon_c(LZL)$—85% decrease in von Mises strain
Cohesive zone model (CZM)	$G_c(LZL)$—85% decrease in normal displacement	$\lambda(LZL)$—85% decrease in normal displacement

$$G_{\mathrm{II}} = \int_0^{\delta_t^p} \tau(\delta_t) d\delta_t \tag{10}$$

where δ_n^p and δ_t^p represent the normal and shear displacements across the adhesive bondline where fracture occurs.

In previous work with elastic DCB specimens, λ was found to equal one. It was hypothesized that, under conditions of extensive adherend plastic deformation, such as in a peel test, the increasing degree of stress concentration at the peel root, reflected by a decreasing LZL, would decrease the adhesive fracture energy, thereby making $\lambda < 1$. The solution procedure was similar to that used with the continuum model: as the peel load on the detached strip was increased iteratively, $\lambda(LZL)$ was calculated at each loading step until it equaled the critical value $\lambda_c(LZL)$ obtained from measured peel data for that adhesive system.

Table 3 summarizes the four combinations of adhesive constitutive model and failure criteria that were investigated. In each case, the approach was the same: 1) Define the failure criterion using the measured peel data; and then 2) quantify the ability of each combination of constitutive model and failure criterion to correlate the measured peel data by predicting the peel loads for the various angles and adherend thicknesses. The errors reported are, therefore, based on the differences between the measured peel forces and the model correlation; *i.e.*, the model predictions.

5. RESULTS AND DISCUSSION

5.1. Continuum Adhesive Model

Figures 5 (a) and (b) show the variation of LZL (85% von Mises stress reduction; *i.e.*, 15% of its value at the root) as a function of the adherend thickness and peel angle for the steady-state peeling of the 1044

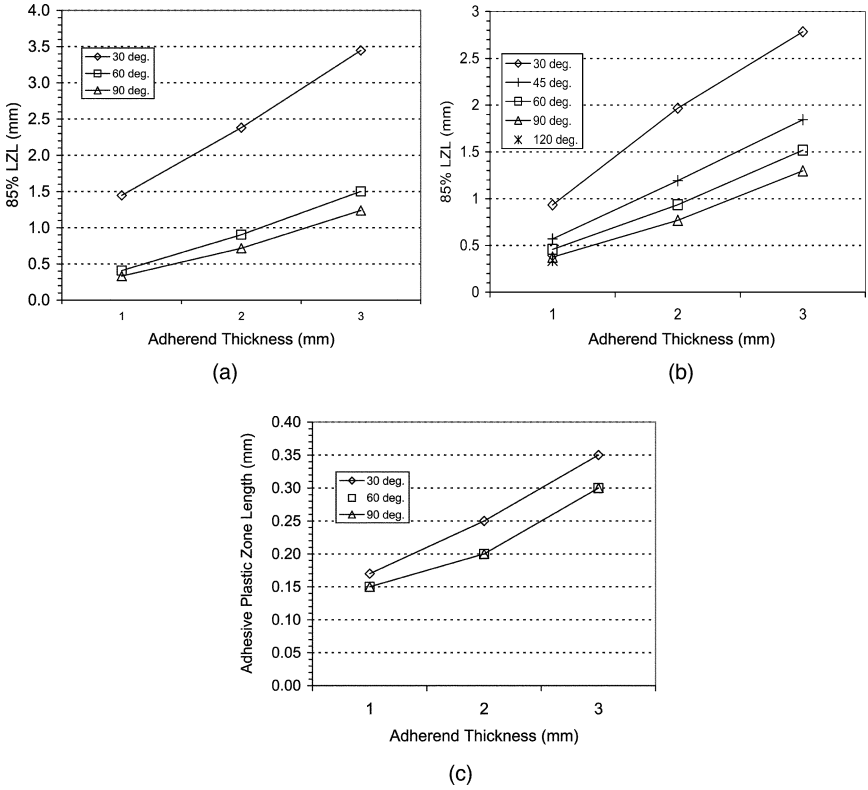

FIGURE 5 *LZL* (85% stress-based definition) from continuum model (uniaxial strain) as a function of peel adherend thickness and peel angle for (a) Betamate 1044 and (b) Betamate 4601 (120° peel angle was only measured with 1-mm sheet). (c) Finite-element prediction of length of adhesive plastic zone for peel data of Betamate 1044 (plane strain) [8].

and 4601 adhesives, respectively. It is seen that, for both adhesives, *LZL* increases almost linearly with the adherend thickness for a given peel angle, reflecting the influence of increasing adherend stiffness in transferring the peel load to a larger volume of adhesive. Similarly, as the peel angle increases for a given adherend thickness, *LZL* decreases as the steady-state peel load becomes increasingly concentrated. The decrease in *LZL* is relatively large in the vicinity of 30° and becomes smaller as the peel angle increases. The smooth variation of *LZL* as a function of thickness and angle contributes to its ability to act as an independent parameter that combines the effects of these two peel properties. Figure 5(c) illustrates that these trends predicted

by the analytical model are consistent with those observed using a nonlinear continuum adhesive finite-element model [8]. In this case, the length of the plastic zone (defined by the von Mises effective yield stress) in the vicinity of the peel root was calculated for each of the nine peel cases measured with the 1044 adhesive [8]. The variation of plastic zone length with peel angle and adherend thickness is very similar to that seen in Figure 5(a) for *LZL* as calculated using the analytical model.

Figures 6(a) and (b) show the $G_c(LZL)$ and $\varepsilon_c(LZL)$ failure criteria, respectively, derived from the measured steady peel loads with the 1044 adhesive by applying the continuum model. Table 1 shows the 1044 peel data and gives the predicted peel forces with the percentage error. It is seen that both G_c and ε_c increase linearly with the length of the load-bearing zone in the adhesive layer; *i.e.*, as the stress concentration (inverse of *LZL*) increases in the adhesive layer, G_c and ε_c decrease. As the adherends become stiffer and the peel angle decreases, *LZL* increases and the behavior of the peel configuration tends toward that of an elastic mixed-mode DCB with much larger values of G_c for a given average phase angle (phase angle averaged over the length of the adhesive layer as described in Ref. 3); for example, at a phase angle of 38°, $G_c = 2{,}000\,\mathrm{J/m^2}$ in a mixed-mode DCB fracture test [8] and approximately $750\,\mathrm{J/m^2}$ for the 1-mm-30 peel test, which has about the same average phase angle. This is due to the direct relationship between the size of the damage zone in the adhesive and the fracture energy; *i.e.*, the elastic DCB produces a larger damage zone and fracture energy than the peel test at the same phase angle because it has a smaller degree of stress concentration. It is noted that *LZL* is not required to define the critical strain energy-release rate in elastic joints because the size of the adhesive damage zone in these cases is essentially independent of the adherend thickness and G_c is only a function of the phase angle.

Figure 6(a) also shows the CZM failure criterion that is discussed later.

Figures 7(a) and (b) show similar results for the 4601 adhesive over a greater number of peel angles. Table 2 lists the 4601 peel data and gives the predicted peel forces with the percentage error.

The predictions of Figures 5, 6, and 7 were obtained assuming a uniaxial state of strain in the adhesive layer ($\varepsilon_x = \varepsilon_z = 0$) and plane strain ($\varepsilon_z = 0$) in the peel strip. As in Ref. 3, this high degree of constraint in the bondline was found to give more consistent results than using either a plane strain or plane stress model for the adhesive. Nevertheless, the trends of the continuum model with each of these failure

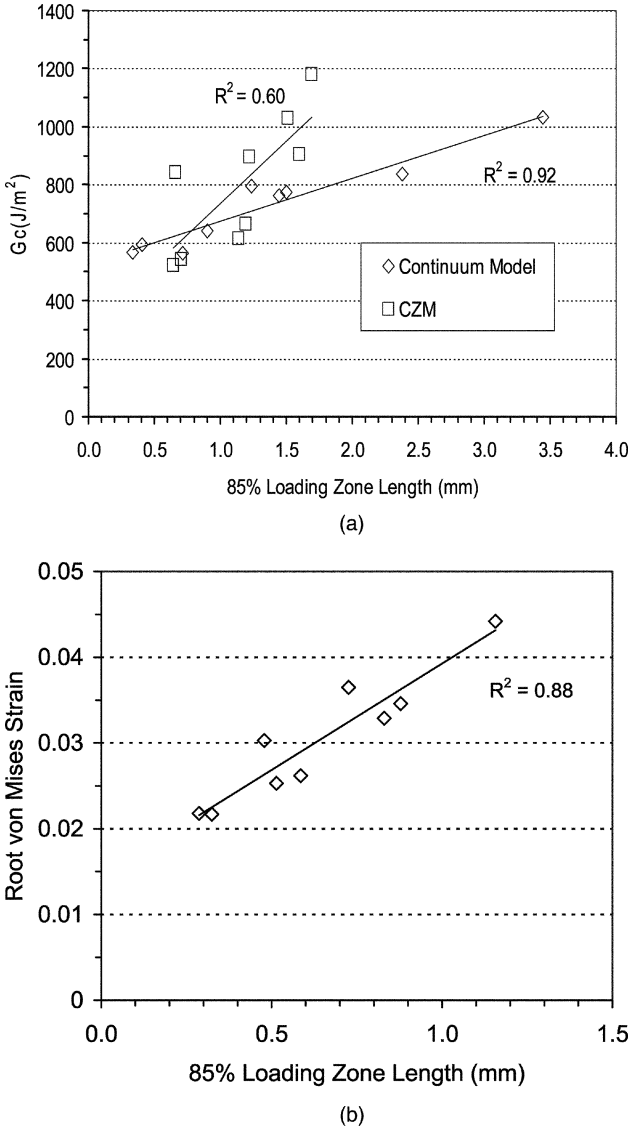

FIGURE 6 Betamate 1044 failure criteria based on continuum model (uniaxial strain) predictions of (a) G_c as a function of loading zone length (85% stress-based definition) and (b) ε_c as a function of loading zone length (85% strain-based definition) using the measured peel data as input (Table 1). Also shown in (a) are the predictions from the cohesive zone adhesive constitutive model as a function of the loading zone length (85% normal displacement definition).

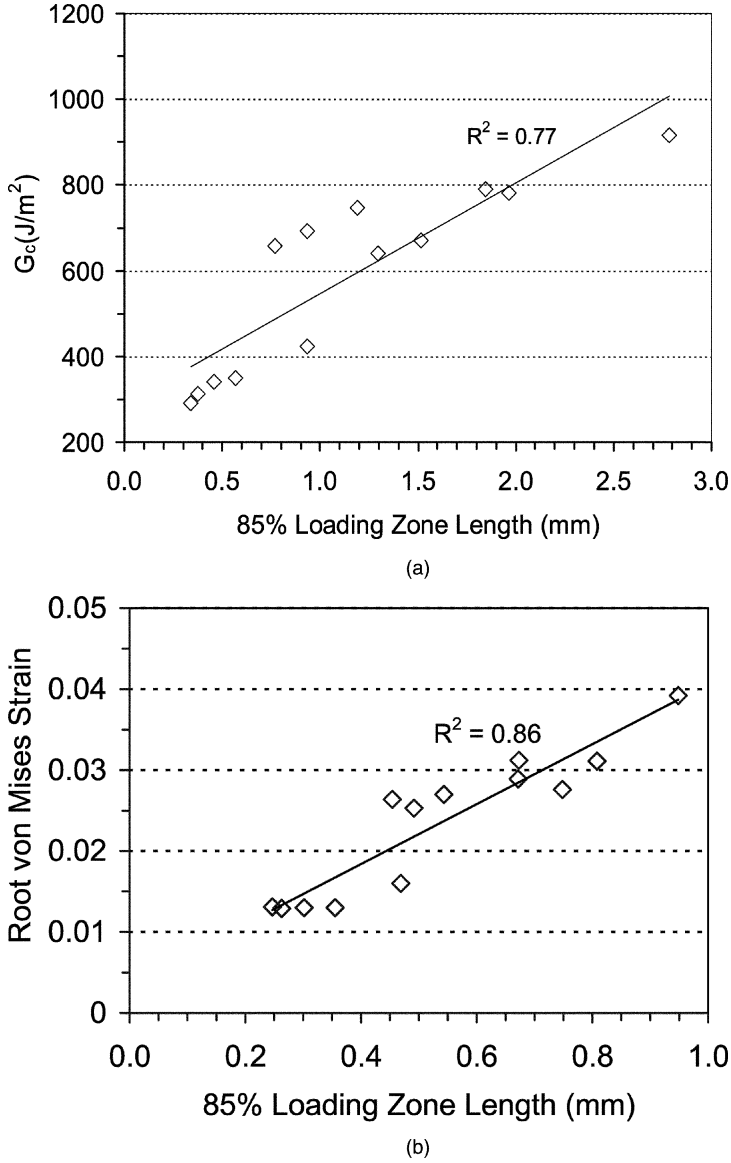

FIGURE 7 Betamate 4601 failure criteria based on continuum model predictions of (a) G_c as a function of loading zone length (85% stress-based definition) and (b) ε_c as a function of loading zone length (85% strain-based definition) using the measured peel data as input Table 2).

criteria were similar regardless of the assumed state of stress in the adhesive layer.

Figures 8(a) and (b) show the measured steady-state peel loads for the 1044 and 4601 adhesives, respectively (Tables 1 and 2), along with the predictions of the continuum model using the $G_c(LZL)$ and $\varepsilon_c(LZL)$ failure criteria [Figure 8(a) also shows the CZM prediction, which is discussed later]. It is seen that both criteria do a reasonable job of predicting the peel load. The prediction errors (listed in Tables 1 and 2 for the continuum model) are summarized in Figures 9(a) and (b) as the average absolute difference between the measured and predicted peel loads over all peel strip thicknesses and peel angles, as well as the range of the maximum and minimum absolute differences. For the 1044 adhesive, the $G_c(LZL)$ and $\varepsilon_c(LZL)$ criteria perform equally well, having an average absolute error of approximately 5% [Figure 9(a)]. The $\varepsilon_c(LZL)$ criteria is best with the 4601 data, giving an average absolute error of approximately 4% [Figure 9(b)]. For both adhesives, the error between the predicted and measured peel forces can be considerably greater than the average in certain cases. Such variation is probably due to scatter in the peel force measurements because the magnitude and sign of the error (Tables 1 and 2) did not appear to be related to any particular peel angle or adherend thickness.

Also shown in Figures 9(a) and (b) are the predictions obtained by defining *LZL* as 1) the length of the adhesive layer subject to a von Mises stress of at least 50% of the value at the root or 2) the length of the adhesive layer subject to a von Mises strain of at least 50% of the value at root. It is seen that the prediction error is relatively insensitive to these changes in the *LZL* definition but is slightly improved using the 85% reduction definitions, which give a longer *LZL*. Similar insensitivity was observed in another trial, this time defining *LZL* in the critical von Mises strain failure criterion as the length from the peel root to the point in the adhesive where the von Mises stress had decreased 85% from its maximum at the root. The results using this *LZL* definition with the 4601 peel data were almost identical to those shown in Figure 9(b) for the $G_c(LZL)$ 85% failure criterion; *i.e.*, approximately 10% greater average absolute error than seen with the strain failure criterion when using the strain-based definition of *LZL*. It is, therefore, concluded that the effectiveness of the $G_c(LZL)$ and $\varepsilon_c(LZL)$ failure criteria with the continuum model are relatively insensitive to the definition of *LZL*.

The values of G_c shown in Figure 6(a) are smaller than those reported in Ref. 3. This discrepancy is due to an error in the computer code of Refs. 2 and 3 in the segment that matched the deformation of the flexible adherend in the sandwich model with that of the detached

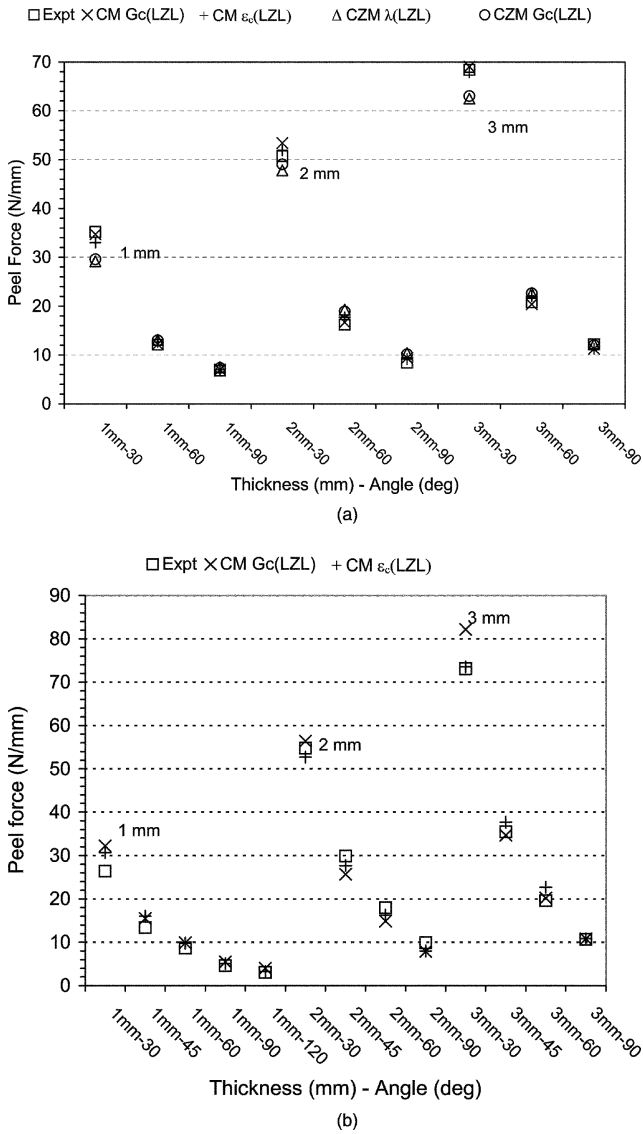

FIGURE 8 Measured and predicted peel forces using the continuum model (CM) and the $G_c(LZL)$ and $\varepsilon_c(LZL)$ failure criteria (85% stress- and strain-based *LZL* definitions, respectively), and the cohesive zone model (CZM) with the $\lambda(LZL)$ and $G_c(LZL)$ failure criteria (85% displacement-based *LZL* definition) for (a) Betamate 1044 and (b) Betamate 4601.

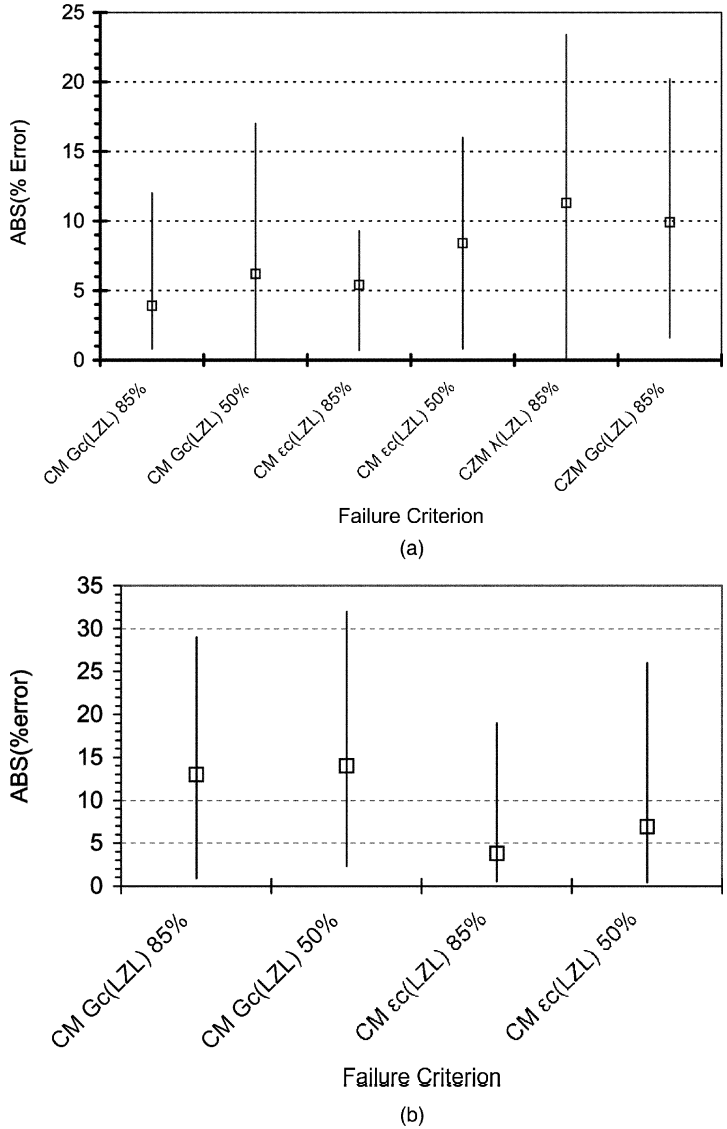

FIGURE 9 Average absolute percentage error in the peel loads predicted by the CM using the $G_c(LZL)$ and $\varepsilon_c(LZL)$ failure criteria and two definitions of LZL, and the CZM using the λ(LZL) and $G_c(LZL)$ failure criteria. Also shown are the errors associated with a different definition of *LZL* in the continuum model (based on the distance for a 50% reduction in von Mises stress or strain). Error bars show the range of the maximum to minimum absolute percentage error: (a) Betamate 1044 and (b) Betamate 4601.

peel adherend. Specifically, the adhesive thickness (0.4 mm) was inadvertently omitted from one of the equations in the code during the calculation of curvature. The sandwich model of Ref. 3 was unaffected; however, the critical von Mises strain and fracture energy calculated from the peel data were incorrect. This error did not have a significant effect on the accuracy of the 1044 peel load predictions in Ref. 3 because the trends of the failure criteria were largely unaffected; only the magnitudes of the strain and energy-release rate were shifted uniformly.

As mentioned previously, it was observed in Ref. 3 that G_c was a linear function of the phase angle, φ, averaged over the entire adhesive layer. This is shown in Figures 10(a) and (b) for the 1044 and 4601 adhesives, respectively, for the continuum model using the 85% stress-based definition of *LZL*. In the present work, an attempt was made to use φ as an independent parameter in the peel force model rather than *LZL*. This led to relatively large errors in the predicted peel force because the $G(\varphi)$ function approaches the $G_c(\varphi)$ failure line very gradually (almost tangentially) as the load applied to the strip is incremented. In comparison, the trajectory of the $G(LZL)$ function approaches and intersects the $G_c(LZL)$ failure line rapidly as the peel load is incremented (Figure 4), making *LZL* a more robust independent parameter in the prediction of the peel force.

By comparing Figures 6, 7, and 10, it is seen that G_c and ε_c vary linearly with both *LZL* and φ. As mentioned earlier, this means that a correlation of G_c and ε_c with *LZL* as an independent parameter is inherently also a correlation with the phase angle, φ. This is consistent with the hypothesis that adhesive failure with yielding adherends should be a function of both the degree of stress concentration at the peel root and the phase angle of the loading.

5.2. Cohesive Zone Model of the Adhesive

As described previously, the traction–separation relations for Betamate 1044 CZM (Figure 3) were determined by applying Equations (6) and (7) to elastic mixed-mode DCB fracture data [9, 10]. The measured mode I and mode II critical energy-release rates were taken to be the areas under the tension and shear curves, respectively (Figure 3); *i.e.*, $\Gamma_{\mathrm{OI}} = G_{\mathrm{Ic}} = 1,680\,\mathrm{J/m^2}$ and $\Gamma_{\mathrm{OII}} = G_{\mathrm{IIc}} = 3,570\,\mathrm{J/m^2}$. The maximum tensile and shear tractions, $\hat{\sigma}$ and $\hat{\tau}$, were determined by modeling the DCB using the adhesive sandwich component of the peel model and adjusting them to give the best fit to mixed-mode DCB fracture data at phase angles of 48° and 69°; *i.e.*, $G_{\mathrm{c48}} = 2{,}340\,\mathrm{J/m^2}$ and $G_{\mathrm{c69}} = 3{,}000\,\mathrm{J/m^2}$, where the phase angle φ of the loading is defined as

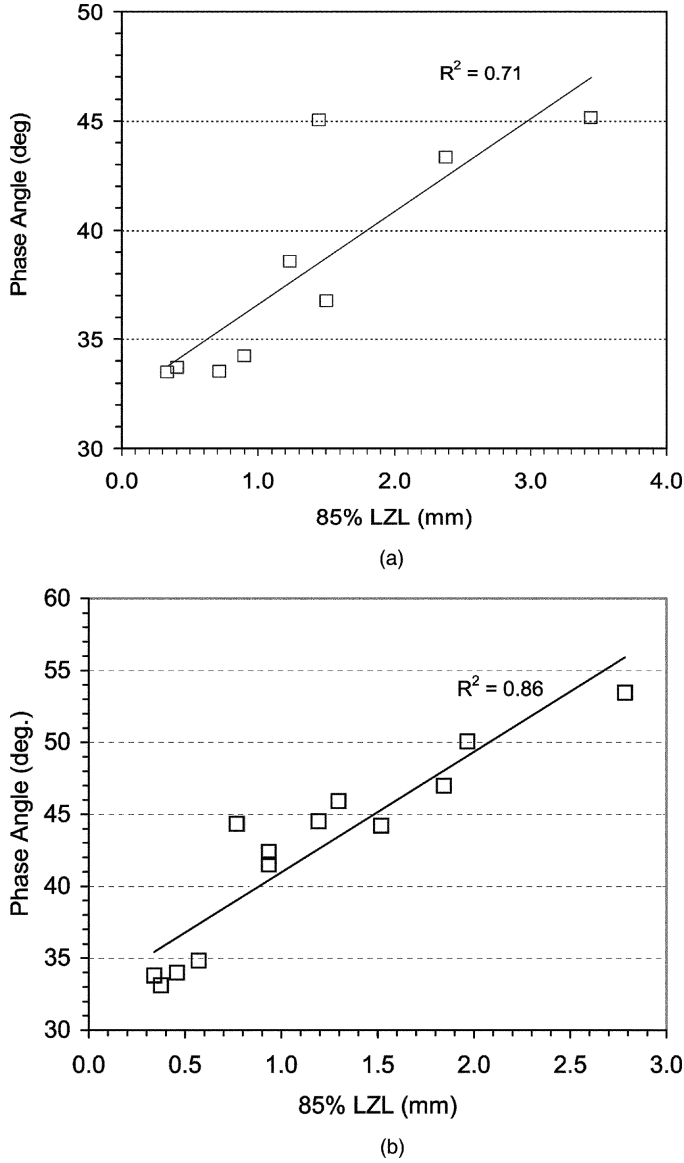

FIGURE 10 Average phase angle as a function of *LZL* (85% stress-based definition, uniaxial strain, continuum model) for (a) Betamate 1044 and (b) Betamate 4601.

TABLE 4 CZM calculations of LZL, G_c, and λ for the Betamate 1044 Peel Data

Adherend thickness (mm)–peel angle (deg)	LZL (mm) 85% reduction in tensile strain	$G_c = G_{\mathrm{I}} + G_{\mathrm{II}}$ ($\mathrm{J/m^2}$)	λ
1–30	0.659	842	0.39
1–60	0.701	542	0.24
1–90	0.642	522	0.23
2–30	1.22	896	0.39
2–60	1.19	664	0.29
2–90	1.14	614	0.26
3–30	1.69	1180	0.48
3–60	1.60	905	0.38
3–90	1.51	1030	0.41

$$\varphi = \tan^{-1}\sqrt{\frac{G_{\mathrm{II}}}{G_{\mathrm{I}}}} \tag{11}$$

The two equations used to specify the unknowns $\widehat{\sigma}$ and $\widehat{\tau}$ are, therefore, Equation (11) and $G_{\mathrm{I}} + G_{\mathrm{II}} = G_c$. This procedure yielded $\widehat{\sigma} = 85.5\,\mathrm{MPa}$ and $\widehat{\tau} = 70\,\mathrm{MPa}$ as the best choices. The resulting traction–separation curves used in the CZM could then predict the 48° and 69° values of G_c with an accuracy of 12% and 20%, respectively. Data were unavailable to construct a CZM for the Betamate 4601 adhesive.

Table 4 lists the values of LZL, G_c, and λ calculated by applying the measured peel forces to this CZM of the tensile and shear behavior of the adhesive layer (Figure 3). As mentioned previously, LZL in this case was defined as the distance from the peel root to the point where the adhesive normal (transverse) displacement (δ_n) was 15% of that at the root. Figure 6(a) shows that the $G_c(LZL)$ CZM failure criterion results in a range of G_c values that is very similar to that obtained from the continuum model. As might be expected, the values of LZL shown in Figure 6(a) resulting from the two definitions (85% stress reduction and 85% normal displacement reduction) are quite different, but this has no bearing on the suitability of the two failure criteria. It is noted in Figure 6(a), however, that the CZM linear correlation $G_c(LZL)$ has more scatter than that for the continuum model.

The CZM was used with two failure criteria—one based on $G_c(LZL)$, the other utilizing $\lambda(LZL)$, where λ is defined by Equation (8). Figure 11 illustrates the variation of λ with peel angle and adherend thickness for the nine 1044 peel cases. The trends are consistent with the hypothesis that λ should decrease, reflecting a decrease in G_c

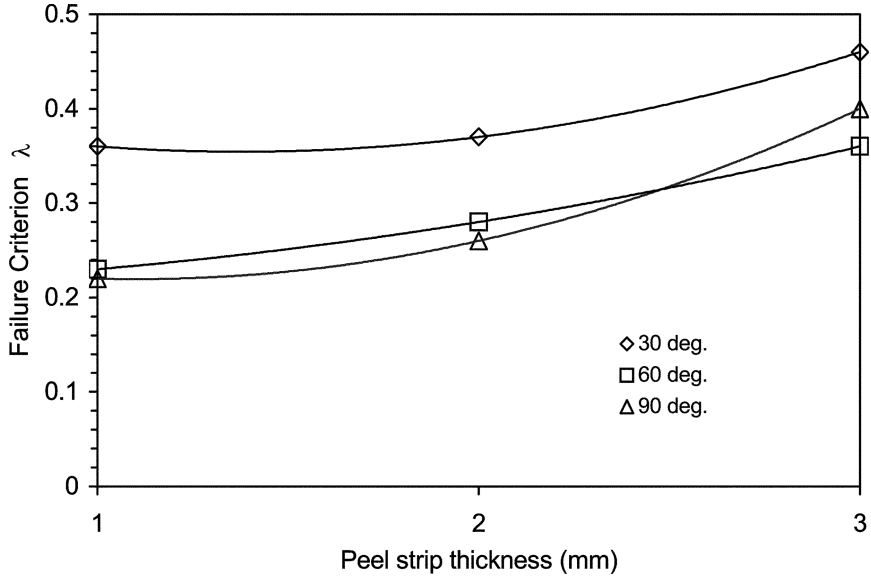

FIGURE 11 Failure criterion, λ, calculated for the Betamate 1044 peel data as a function of the peel strip thickness and the peel angle.

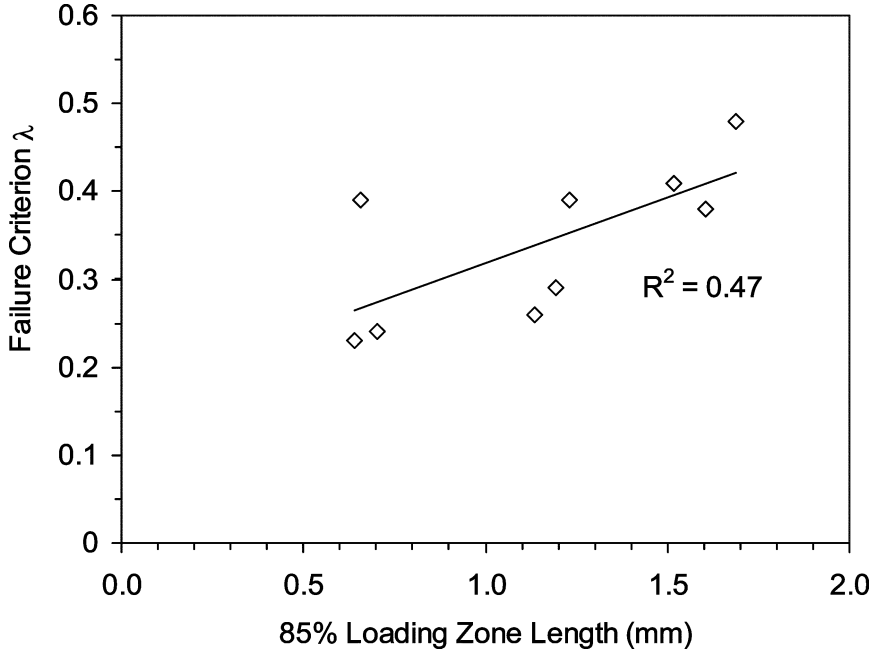

FIGURE 12 Failure criterion, λ, as a function of the *LZL* (85% definition) for Betamate 1044.

[Equation (8)], as the stresses become more concentrated at the peel root. For example, λ tends to decrease with increasing peel angle and decreasing adherend thickness. Figure 12 reflects this trend in terms of the variation of λ with *LZL*, although the linear correlation has considerable scatter. This may be due to the inherent inaccuracy of the CZM model, because the $G_c(LZL)$ correlation of Figure 6(a) also displayed more scatter than the continuum model.

Using these two CZM failure criteria [$G_c(LZL)$ in Figure 6(a) and $\lambda(LZL)$ in Figure 12], the CZM model was used to predict the steady-state peel loads for the 1044 adhesive. Figure 9(a) shows that the average absolute error and the range of the absolute errors for the $\lambda(LZL)$ failure criterion was larger than those obtained with the various failure criteria used with the continuum model. The CZM $G_c(LZL)$ failure criteria produced very similar results; *i.e.*, an average absolute error of 10% with a range of 20% to 2%.

6. CONCLUSIONS

An analytical model for the stresses in the adhesive layer of a flexible–rigid peel specimen has been modified to use the adhesive "loading zone length" (LZL) as an independent parameter. In this context, *LZL* is a measure of the length of the loaded adhesive layer in the vicinity of the peel root, and as such incorporates the effects of the peel angle, adherend thickness, and the mechanical properties governing the elastic and plastic deformation of the adhesive and adherend. It was observed that *LZL* varied linearly with the average phase angle of the loading and, therefore, encompassed the effects of both the mode ratio of loading and the degree of stress concentration at the peel root.

The analytical model can be constructed using either of two constitutive models for the adhesive: 1) an approximate continuum model or 2) a cohesive zone model in which the tensile and shear behavior of the adhesive was mimicked using two traction–separation relations. For the continuum model, it was observed that the measured peel data for both adhesives could be correlated using *LZL* as the independent parameter with either a critical strain energy failure criterion or one based on the critical von Mises strain at the peel root; the average absolute error in the correlations was between 3% and 13% depending on the criterion and the adhesive. The constitutive properties of the CZM were defined using mixed-mode DCB fracture energies. Two strain energy–based failure criteria were evaluated with the CZM, with each producing an average absolute error in the correlation of about 12%.

The present experiments were conducted using one adhesive thickness. Experience with mixed-mode DCB fracture tests [1, 9] suggests that that the same trends would be seen with other thicknesses, and that the $G_c(LZL)$ and $\varepsilon_c(LZL)$ failure criteria are probably relatively insensitive to adhesive thickness.

A copy of the source code, which must be compiled with the required IMSL FORTRAN routines, is available from the corresponding author via email (spelt@mie.utoronto.ca).

ACKNOWLEDGMENTS

The authors gratefully acknowledge the support of Alcan International Ltd., Essex Specialty Products Inc., Henkel Surface Technologies, and the Centre for Automotive Materials and Manufacture, Kingston, Ontario.

REFERENCES

[1] Fernlund, G., Papini, M., McCammond, D., and Spelt, J. K., *Compos. Sci. Tech.* **51**, 587–600 (1994).
[2] Wang, R. X., Cui., J., Sinclair, A. N., and Spelt, J. K., *J. Adhes.* **79**, 23–48 (2003).
[3] Wang, R. X., Sinclair, A. N., and Spelt, J. K., *J. Adhes.* **79**, 49–66 (2003).
[4] Georgiou, I., Hadavinia, H., Ivankovic, A., Kinloch, A. J., Tropsa, V., and Williams, J. G., *J. Adhes.* **79**, 239–265 (2003).
[5] Blackman, B. R. K., Hadavinia, H., Kinloch, A. J., and Williams, J. G., *Int. J. Fracture* **119**, 25–46 (2003).
[6] Shaganpur, A., "Adhesive Joint Failure: Effects of Strain Rate, Temperature and Adherend Yielding," M.A.Sc. Thesis, University of Toronto, 2003.
[7] Crocombe, A. D. and Bigwood, D. A., *J. Strain Analysis* **27**, 211–218 (1992).
[8] Cui, J., Wang, R. X., Sinclair, A. N., and Spelt, J. K., *Int. J. Adhes. Adhesives* **23**, 199–206 (2003).
[9] Fernlund, G. and Spelt, J. K., *Compos. Sci. Tech.* **50**, 441–449 (1994).
[10] Sareskani, S., "Adhesive Failure with Adherend Yielding—the T-Peel Test and Cohesive Zone Modeling," M.A.Sc. Thesis, University of Toronto, 2003.